Hindawi
Advances in Materials Science and Engineering
Volume 2020, Article ID 7869345, 9 pages
https://doi.org/10.1155/2020/7869345

Research Article

Characterization Methods for the Effect of Microbial Mineralization on the Microstructure of Hardened C_3S Paste

Yanqiang Chen,[1,2,3,4] **Chunxiang Qian**,[1,2,3,4] **and Hengyi Zhou**[1,2,3,4]

[1]*School of Materials Science and Engineering, Southeast University, Nanjing 211189, China*
[2]*Research Center of Green Building & Construction Materials, Southeast University, Nanjing 211189, China*
[3]*Key Laboratory of Materials Microbiology, Southeast University, Nanjing 211189, China*
[4]*Jiangsu Key Laboratory of Construction Materials, Southeast University, Nanjing 211189, China*

Correspondence should be addressed to Yanqiang Chen; 230169462@seu.edu.cn and Chunxiang Qian; cxqian@seu.edu.cn

Received 3 May 2020; Accepted 14 July 2020; Published 18 August 2020

Guest Editor: Sreekanta Das

Microbial mineralization has a significant effect on the hydration process of cement-based materials. This paper mainly studied the characterization methods for hydration degree and hydration product of C_3S in hardened paste under microbial mineralization. Quantitative X-ray diffraction (QXRD), thermogravimetric analysis (TG), Fourier transform infrared spectroscopy (FT-IR), and electron backscatter diffraction (EBSD) were used and compared. The results showed that microbial mineralization increased the hydration degree of T-C_3S. QXRD and EBSD could be used to characterize the content of C_3S, and there were few differences between the two methods. TG could accurately characterize the content of $Ca(OH)_2$ and $CaCO_3$ at different depths of the sample, and FT-IR could qualitatively characterize the presence of $Ca(OH)_2$ and $CaCO_3$.

1. Introduction

In recent years, microbial mineralization in cement-based materials has become a research focus. Microbial-induced calcium carbonate precipitation (MICCP) [1, 2] is a typical biomineralization process which could be used to heal cracks in concrete and enhance the durability of cement-based materials [3]. In addition, new microbial cement-based materials have also been developed [4]. However, the effect of microbial mineralization on cement-based materials was caused by the effect on hydration process. Therefore, it was necessary to study the hydration and its characterization methods.

Many traditional methods for characterizing the hydration process of cement-based materials, such as heat evolution method, quantitative XRD (QXRD), differential thermal analysis (TGA), BSE, and so on, were used frequently. However, each method had its limitations.

Peiming et al. [5] compared the advantages and disadvantages of hydration heat method, chemically combined water method, $Ca(OH)_2$ quantitative test method, and BSE method; the results showed that the BSE method had a better promising application for the characterization of hydration degree. Kocaba et al. [6] studied the degree of hydration of cement-based materials mixed with blast furnace slag and showed that it was poor to characterize the degree of hydration by the dissolution method and TGA method, while the results of image analysis and isothermal calorimetry were highly consistent. Alexander [7] compared the XRD and BSE methods to characterize the phase composition of the hardened paste, and the results showed that the two characterization methods were also highly consistent.

Microbial mineralization consumes $Ca(OH)_2$ in the hardened paste; therefore, the mineralization of microorganisms was closely related to the hydration process of the paste. Basaran Bundur [8] studied the effect of *S. pasteurii* bacteria on the hydration process of cement-based materials by hydration heat method and showed that there was a great effect of *S. pasteurii* bacteria on the hydration heat of mortar. Lee [9] also used hydration heat method and XRD method to

characterize the effect of bacteria on the hydration of cement-based materials. The results showed that the former method could clearly characterize the early-phase change of the hydration process caused by bacteria, and the latter could characterize the composition change of the phase during the whole hydration process. But for the intermediate products, the limitations were obvious.

Microbial mineralization could affect the hydration process and microstructure of cement-based materials by promoting the transformation of Ca $(OH)_2$ to $CaCO_3$. However, the characterization methods of cement hydration under mineralization lacked systematic research. Therefore, in order to systematically characterize the effects of mineralization on cement hydration, this paper mainly discussed the changes in the degree of hydration and products of hardened C_3S paste caused by mineralization through different characterization methods and compared the advantages and disadvantages of different characterization methods. The combination of different characterization methods could more accurately characterize the mineralization and hydration processes. In addition, the results of the study will provide a better understanding of mineralization and guide engineering practice.

2. Materials and Experimental Design

2.1. Raw Materials

2.1.1. Tricalcium Silicate. Before the test of C_3S sample, the C_3S powder was grinded to below 200 mesh in a dry environment for testing. The XRD pattern of C_3S which was collected using a D8-Discover diffractometer (Brook, Germany) is shown in Figure 1. The phases of the samples were mainly C_3S and CaO. By comparing C_3S crystal standard cards, it was concluded that the crystal form was T-C_3S. Fitting was calculated by TOPAS software [10]; the purity of C_3S was about 99.05%. The C_3S particle size distribution is shown in Figure 2. The particle size of the sample ranged between 3.62 and 70.4 μm, and the average particle size was 13.68 μm. Before the XRF test, the C_3S powder and boric acid were added to the pressure equipment and compressed into a tablet, and the element of C_3S by XRF (ARL Perform X 4200, Thermo Fisher) is shown in Table 1. In addition to CaO and SiO_2, it also contained a small amount of MgO, Al_2O_3, etc., and the ratio of CaO to SiO_2 was 3.04. The specific surface area was 388.29 m^2/kg.

2.1.2. Microbial Culture. *Paenibacillus* was selected and used in the study. Before experiment, *Bacillus* were domesticated for half a year in an alkaline environment. Medium for culture of the microorganisms is shown in Table 2, and the pH of the medium was adjusted by $Ca(OH)_2$. After the medium was autoclaved at 121°C for 25 min, the bacteria were inoculated into it, and then the inoculated medium was placed in a shaking incubator with an oscillation frequency of 170 r/min and cultured at 30°C for 24 hours. The bacterial growth curve is shown in Figure 3, and the pH of the medium was 12. After 24 hours of culture, the number of bacteria measured by flow cytometry (ACEA D2040R, China) was 2.0×10^8 cells/mL.

2.2. Biomineralization Experiment Design. In order to characterize the effects of biomineralization on the hydration degree and products of cement-based materials, a set of comparative experiments of mineralization and carbonization was designed. The microbes in the form of a suspension were mixed with C_3S powder. The number of microbes added was calculated based on the volume of the suspension. The amount of microorganism suspension added was equal to mixing water. The water–cement ratio was 0.45, the curing temperature was 20 ± 0.5°C, relative humidity was 65 ± 5%, the CO_2 concentration was 0.012 mol/L, and the curing time was 7 d. The schematic diagram of the test process is shown in Figure 4.

2.3. Characterization Methods

2.3.1. Characterization of Crystal Form and Phase Content by QXRD. QXRD was used to quantitatively analyze the crystal form and phase content of cement components. In the XRD quantitative analysis process, in order to reduce the data error, obtaining a higher-quality XRD map was necessary. During fitting the map, the number of the phases selected was gradually increased, so that the error was reduced. In addition, the preferred orientation of the phase was adjusted until the fitting map was similar to the one tested. The QXRD pattern was collected using a D8-Discover diffractometer (Brook, Germany) with a target source of Cu Kα, voltage and current of 40 kV and 30 mA, scan range of 10°–90°, and step size of 0.002°, 0.35 seconds per step. Quantitative analysis was performed by Bruker's Topas Version 4.2 software [10], and a monoclinic structure of C_3S described by Nishi [11] was used. In the process of quantitative analysis, Rwp was used as an indicator of the degree of software fitting and was also the standard of accuracy of the results. In this study, the values of Rwp were between 8.11 and 11.04, which was less than 15. Therefore, the results of Topas 4.2 calculations were credible [10].

When preparing test samples, the C_3S hardened paste was measured and sized the upper layer of the test piece within 7 mm by using a caliper. The label was marked every 1 mm, and then the sample was polished with a file. Multiple measurements were taken to ensure the evenness of the hardened paste and the accuracy of the sampling depth. During samples preparation, all errors did not exceed 0.1 mm. The schematic diagram is shown in Figure 5. The powder sample obtained was further ground and then immersed in absolute ethanol solution for 3 days to arrest hydration and then dried in a vacuum oven at 60°C for 3 days. Before the test, α-Al_2O_3 with a mass fraction of 10% was added as an internal standard and uniformly mixed.

2.3.2. Quantitative Analysis of the Content of $CaCO_3$ and $Ca(OH)_2$ at Different Depths. TG was used to determine the $Ca(OH)_2$ and $CaCO_3$ content in the samples. The equipment used was Netzsch STA 449 F3. 5–10 mg of sample powder was placed in a Pt/Rh crucible and heated to 1000°C at 10 K/

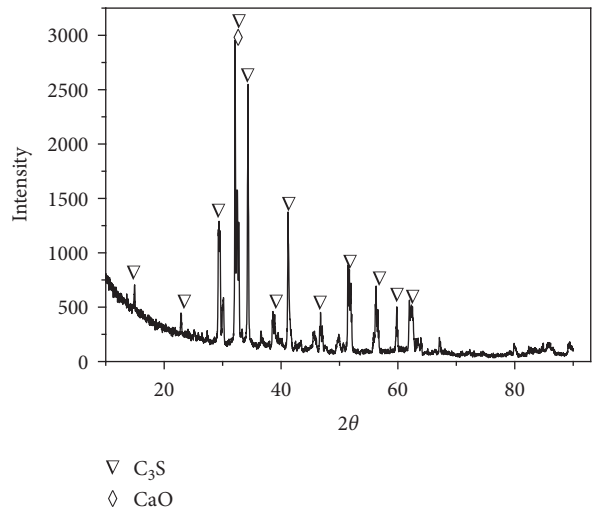

Figure 1: XRD pattern of C_3S.

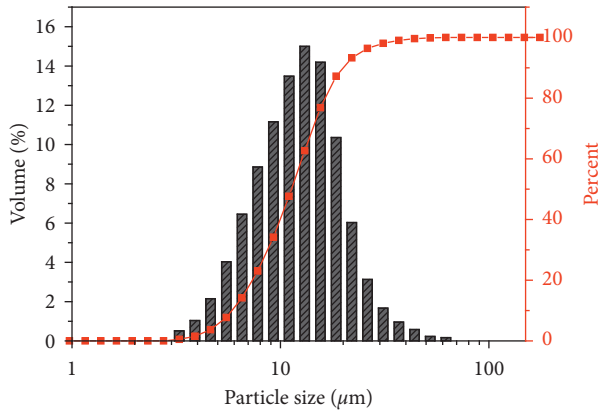

Figure 2: Particle size of C_3S.

Table 1: Chemical composition of C_3S samples by XRF analysis.

Oxide	CaO	SiO_2	MgO	Al_2O_3
Content (%)	75.07	24.60	0.15	0.07
Total (%)		99.89		

min in an N_2 atmosphere. The mass percentages of $Ca(OH)_2$ and $CaCO_3$ were calculated from the weight loss rate in the thermogravimetric curve. The analysis methods of TG curve mainly included "tangent method" and DTG. Younsi [12] pointed out that the $Ca(OH)_2$ content measured by the "tangent method" was about 20% lower than the actual value, so the analysis method used in this study was DTG.

The sample preparation for TG test was similar to that for XRD test, besides that no α-Al_2O_3 was added in TG.

2.3.3. EBSD-EDS Characterizing Phase Content. For EBSD imaging, the reaction of C_3S with water during hydration made the average number of atoms much lower than that of the unhydrated C_3S particles, so a strong difference of gray-scale was obtained between unreacted (anhydrous) and reaction products (hydrates). Based on the entropy

Table 2: *Paenibacillus* medium.

Nutrients	Liquid medium (g/L)
Sucrose	10.0
$Na_2HPO_4{\cdot}12H_2O$	2.50
$MgSO_4$	0.50
$CaCO_3$	1.00
KCl	0.15
$(NH_4)_2SO_4$	0.50
Yeast extract	0.30

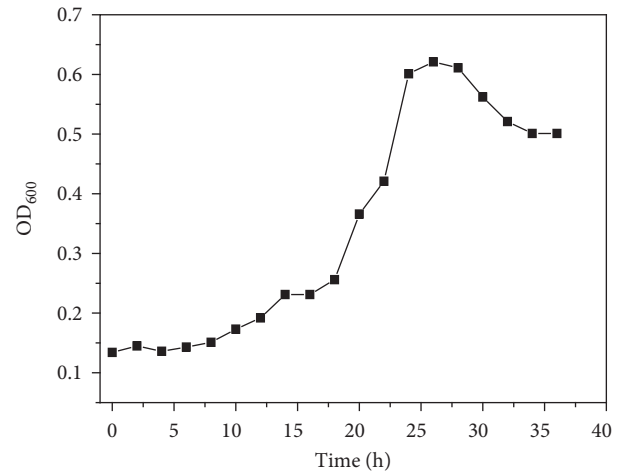

Figure 3: The growth curve of *Paenibacillus* (pH = 12).

maximization of the GLH curve, image processing was performed by image processing software (Image-Pro Plus 6.0) to extract the area fraction of the gray value. Regarding the processing of the image: first, the threshold of the entropy maximization of the GLH curve was obtained from plurality of images, and then a binary grayscale range image was obtained corresponding to the C_3S hardened paste. In addition, the microscope was operated at an acceleration voltage of 15 kV. Images of each sample were collected at magnifications of 250 × (20 fields), 500 × (30 fields), and 1000 × (50 fields).

Before the test, the samples were impregnated with epoxy resin and polished, and then the equipment was sprayed with carbon 360 nm using the equipment LEICA ACE600 and then photographed by using a backscattered scanning electron microscope.

2.3.4. FT-IR Qualitative Characterizing Phase. FT-IR was frequently used to characterize functional groups in samples. The principle was that when the sample was irradiated with infrared light with a continuously changing frequency, the molecules absorbed radiation at certain frequencies, so that the intensity of the transmitted light in the absorption region was weakened. The infrared spectrum was obtained by recording the relationship between the percentage transmittance of infrared light and the wave number or wavelength. The device model used during the test was Nicolet iS10, with a spectral range of 500 cm^{-1}–4000 cm^{-1} and the resolution better than 0.4 cm^{-1}. This method was mainly used for the characterization of $Ca(OH)_2$ and $CaCO_3$.

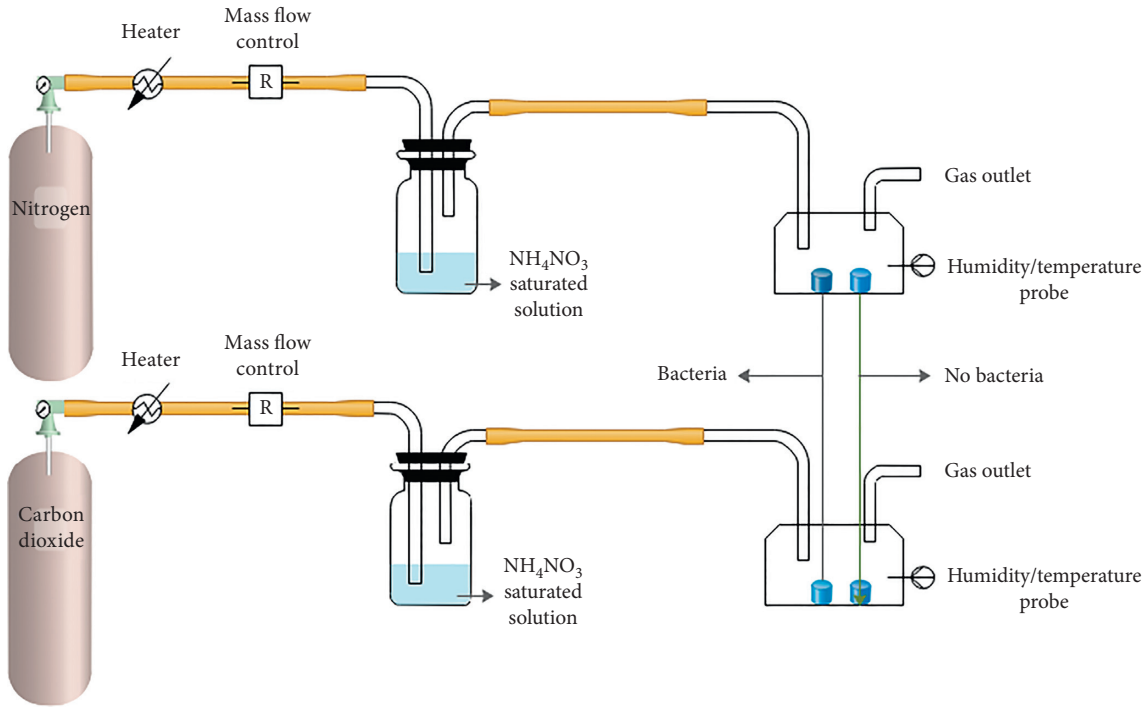

Figure 4: Schematic diagram of mineralization/carbonization setup.

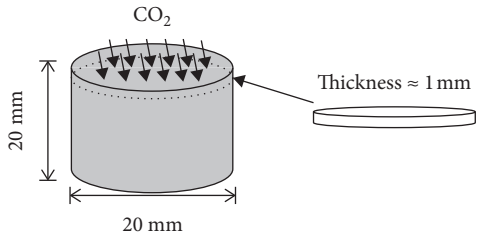

Figure 5: Schematic diagram of sample processing.

3. Results and Discussion

3.1. Characterization of Crystal Form and Phase Content by QXRD. XRD test was performed on mineralized and carbonized samples at different depths. The results within about 1 mm of the surface layer are shown in Figure 6. Among them, B was the mineralization group and C was the carbonization group (the same applies hereinafter). From the figure, there was a significant difference in the peak intensity near 29.4°, and by comparing the crystal forms, it was analyzed as calcite, indicating that the crystallinity of $CaCO_3$ within 1 mm of the surface layer of the mineralized group was better than that of the carbonized group. In addition, it could be seen from the figure that there was no peak at 18.4° within 0-1 mm of the surface layer, indicating that the $Ca(OH)_2$ was completely mineralized or carbonized in the previous period.

Through Topas software, quantitative analysis of XRD patterns of T-C_3S hardened paste at different depths is shown in Figure 7. As shown in Figure 7, the residual amount of C_3S in the mineralization group samples was lower than that of the carbonization group at different depths, indicating that the addition of microorganisms promoted the hydration of C_3S. It was known from the literature that the decrease in C_3S content in mineralized samples might be related to bacteria as nucleation sites and then promote hydration. The above tests showed that QXRD could be used to characterize the degree of hydration of cement-based materials and perform phase analysis.

3.2. Quantitative Analysis of the Content of $CaCO_3$ and $Ca(OH)_2$. TG test was performed at different depths within surface layer of the mineralization group and the carbonization group, and the curve is shown in Figure 8. By analyzing and calculating the TG curve in Figure 8, the content of $Ca(OH)_2$ and $CaCO_3$ at different depths was obtained, as shown in Figure 9. It could be seen that $CaCO_3$ in the mineralized group was higher than that in the carbonized group, which indicated that the mineralization promoted the formation of $CaCO_3$. From the curve of $Ca(OH)_2$ in Figure 9, it was concluded that within 4 mm of the surface layer, the content of $Ca(OH)_2$ was lower than the carbonization group. This was due to $Ca(OH)_2$ mineralized to $CaCO_3$. In 4–7 mm, the content of $Ca(OH)_2$ in the mineralized group was higher than that in the carbonized group, that is, the mineralization promoted the hydration of C_3S, and more $Ca(OH)_2$ was produced, which was consistent with the results of QXRD. In addition, from Figure 8, the weight loss of the mineralized group and the carbonized group at 1000°C was slightly different within the range of 0–2 mm, the weight loss of the mineralized group was slightly higher than that of the carbonized group. The reason was that mineralization promoted the reaction between CO_2 and $Ca(OH)_2$, so the weight loss rate of the mineralized group was high.

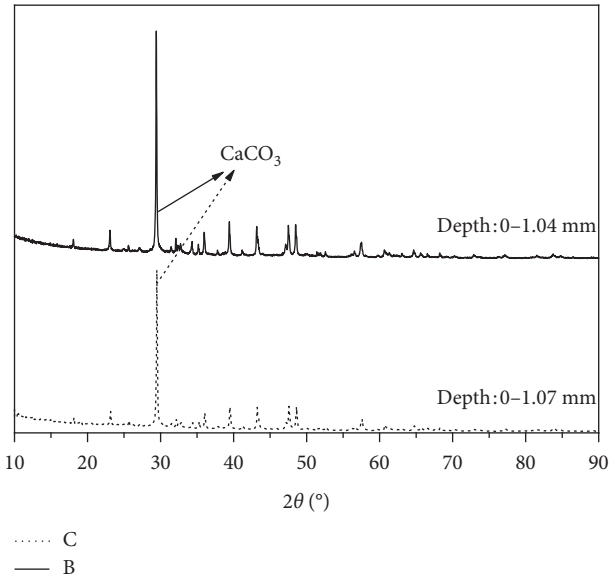

Figure 6: Comparison of $CaCO_3$ peak intensity within about 1 mm of the surface layer.

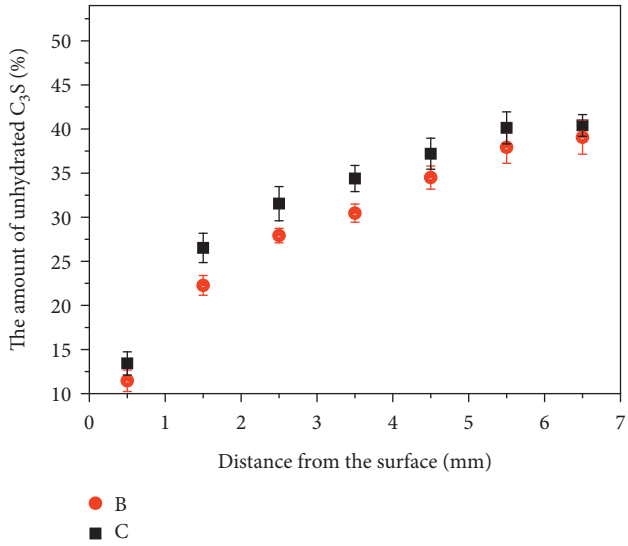

Figure 7: Remaining amount of C_3S at different depths in the surface layer.

3.3. EBSD-EDS Characterization of the Content of the Phases. By cutting the samples longitudinally and then performing BSE shooting at different magnifications, as shown in Figure 10. The magnification used in this test was ×250 for statistics and ×1000 for analysis.

At a magnification of ×250, more than three photos were taken. The software Image-Pro Plus 6.0 was used to analyze the grayscale of photos. Figure 11 shows the grayscale distribution of BSE images under this test conditions. Combining the energy spectrum and the literature, it could be seen that the first peak corresponds to the pore, the second peak corresponds to the phase C-S-H, the third peak corresponds to the phase of $Ca(OH)_2$ and $CaCO_3$, and the fourth peak corresponds to the unhydrated particles. The threshold was further determined according to Figure 12.

From Figure 12, it was concluded that the Ca/Si in region I was about 3, which was unhydrated C_3S; in region II, the Si content was close to 0, which was $Ca(OH)_2$ and $CaCO_3$. From Figure (c), it could be concluded that the grayscale values at I, II, and III were greatly different when passing through different grayscale areas at the line scanning, and the grayscale values changed greatly at the connection points. Combining the gray distribution of the whole picture, area I was unhydrated C_3S, area II was $Ca(OH)_2$ and $CaCO_3$, and area III was C-S-H and some pores.

Combining the above methods, rendering was performed at different gray values, as shown in Figure 13.

Combined with the literature, it was calculated that the C_3S content of the surface layer of the mineralization group within the range of 0-1 mm was $11.30 \pm 1.64\%$, and the content of $Ca(OH)_2$ and $CaCO_3$ was $67.34 \pm 1.49\%$. The porosity was $21.36 \pm 2.19\%$; the C_3S content in the 0-1 mm surface layer of the carbonization group was $14.1 \pm 1.24\%$, and the content of $Ca(OH)_2$ and $CaCO_3$ was $60.17 \pm 1.19\%$. The porosity was $25.73 \pm 1.98\%$. The above data showed that microbial mineralization promoted the hydration of T-C_3S, which was consistent with the QXRD test results. In addition, the mineralization of microorganisms reduced the porosity of the surface layer.

3.4. FT-IR. In the T-C_3S hardened paste of the mineralization group and the carbonization group, a small amount of samples was taken at different depths for FT-IR testing. The results are shown in Figure 14.

In Figure 14, the vibrational peak at a wavelength of 3443 cm^{-1} represents –OH, and the vibrational peak at a wavelength of 713 cm^{-1}, 874 cm^{-1}, and 1797 cm^{-1} represents CO_3^{2-}. It could be seen that within 0–3 mm, the peak value of the sample in the mineralization group at 874 cm^{-1} was more obvious than that of the carbonization group. It reflects

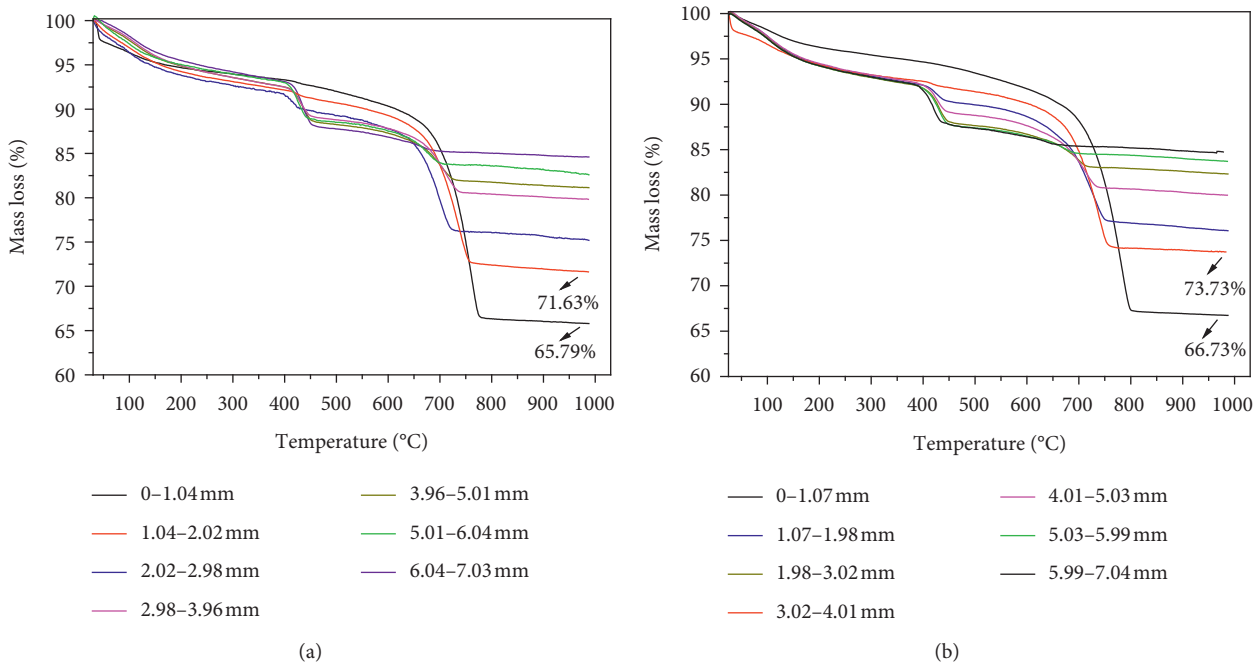

Figure 8: Mass loss curves at different depths of samples in the mineralization group (a) and the carbonization group (b).

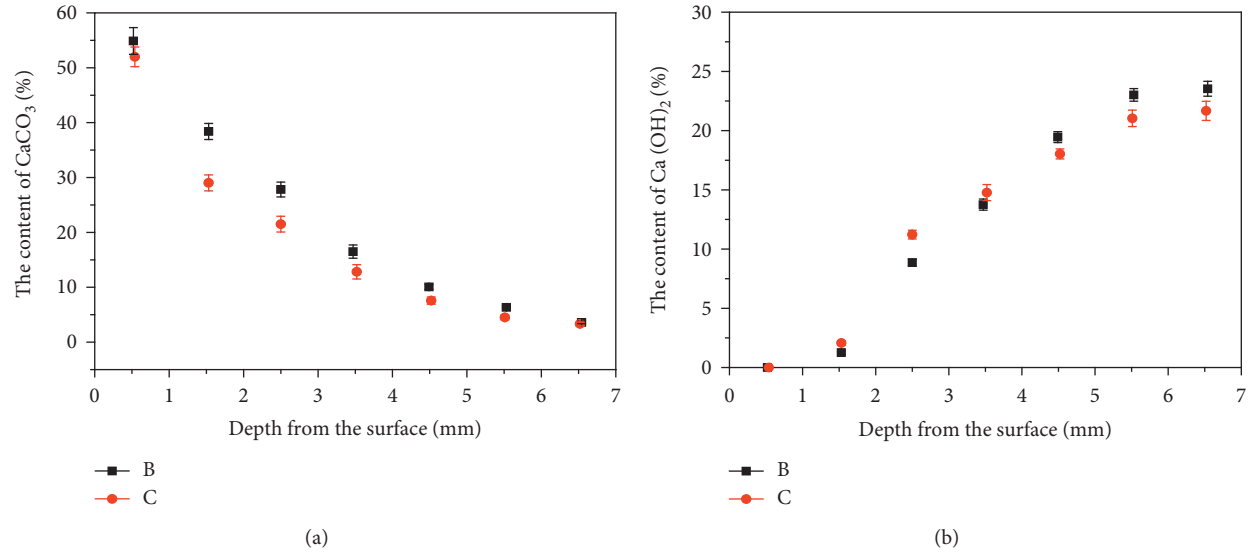

Figure 9: Content of $CaCO_3$ (a) and $Ca(OH)_2$ (b) at different depths of samples.

that the addition of microorganisms promoted the formation of $CaCO_3$ to some extent.

3.5. Comparisons. By combining the four characterization methods of QXRD, TG, EBSD, and FT-IR, the morphology, phase content, porosity, and main functional groups of cement-based materials with microbial mineralization could be obtained. QXRD, TG, and EBSD could quantitatively characterize the phases, while the results of FT-IR were qualitative. Because of the good fitting effect of QXRD results on crystal, it could be used to quantify the content of C_3S. However, the fitting results of $Ca(OH)_2$ were lower which actually were due to its amorphous phase. TG could accurately determine the contents of $Ca(OH)_2$ and $CaCO_3$ according to the loss of combustion.

Different phases could be distinguished according to the gray value by EBSD. The quantitative results of C_3S content in the mineralized surface obtained by comparing EBSD and QXRD are shown in Table 3. It could be seen that for the C_3S content within 0-1 mm of the surface layer of the mineralization group and the carbonization group, the results obtained by the two characterization methods were relatively

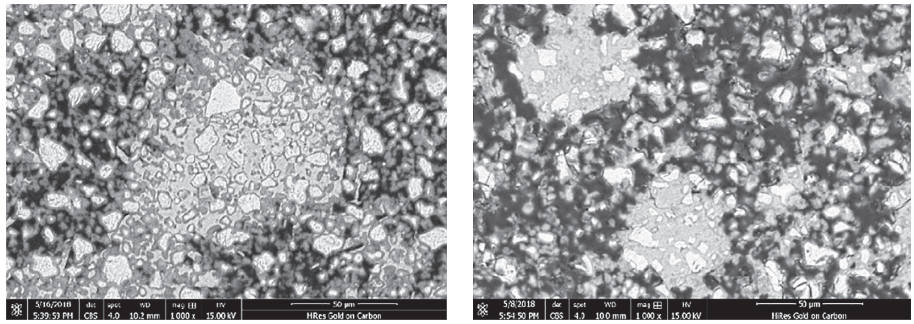

(a) (b)

Figure 10: BSE image of the surface layer of the mineralization group (a) and carbonization group (b) (0~1 ± 0.3 mm).

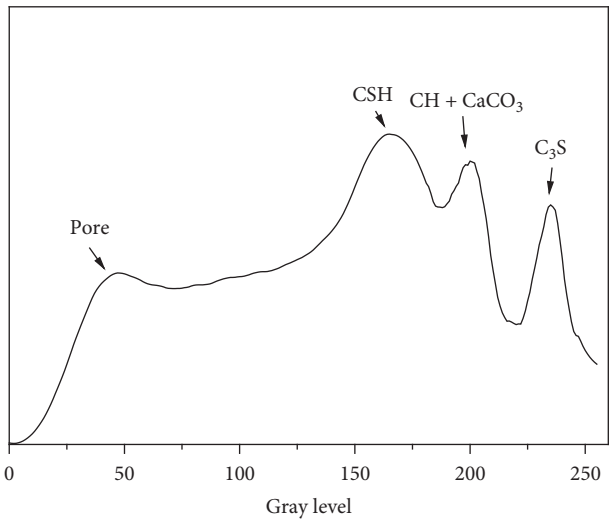

Figure 11: Gray distribution of BSE images of the BSE images.

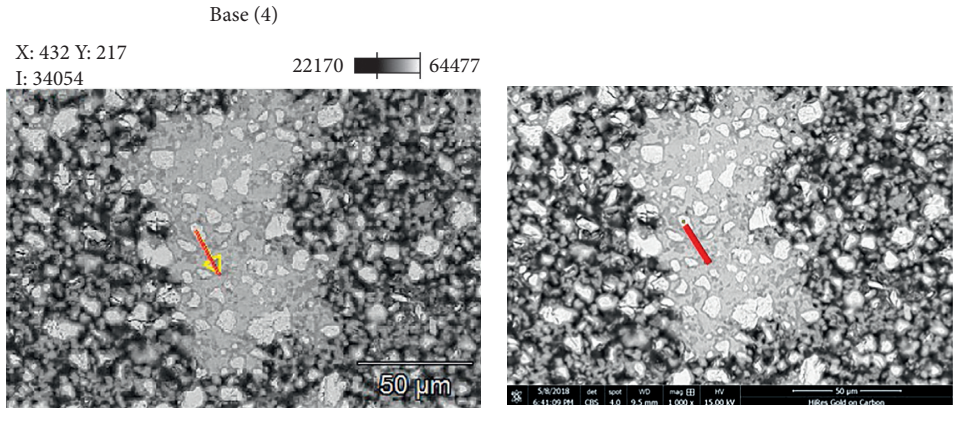

(a) (b)

Figure 12: Continued.

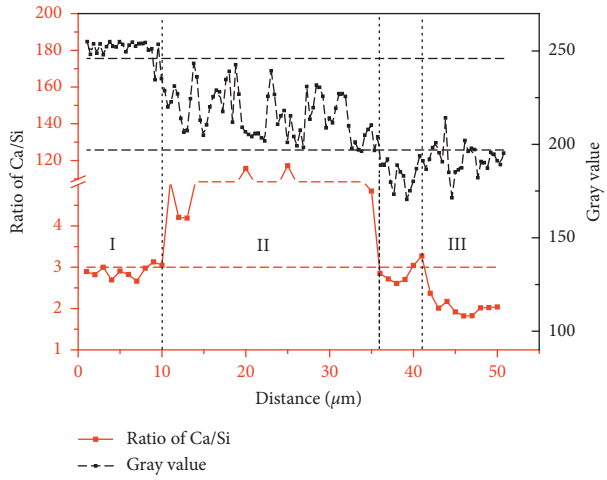

(c)

Figure 12: Corresponding map of BSE gray distribution and EDS. (a) The original line scan. (b) Postproduction, in order to facilitate observation and analysis. (c) The map of Ca/Si and gray value.

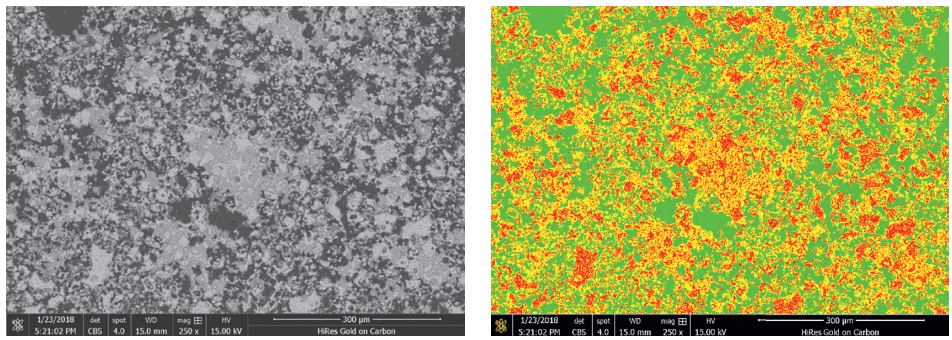

(a) (b)

Figure 13: Color rendering of the EBSD picture based on the gray value.

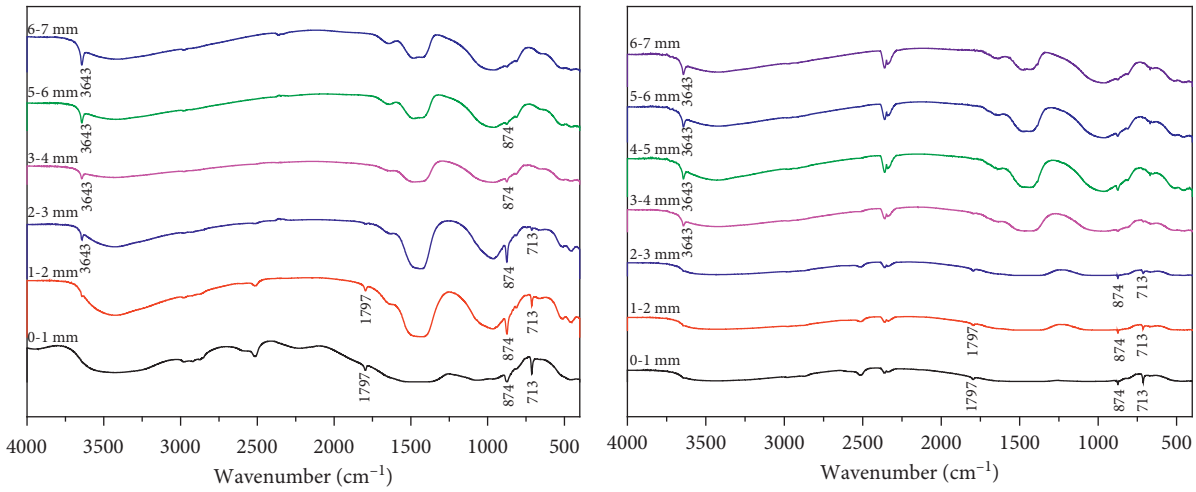

(a) (b)

Figure 14: Infrared curves of samples in the mineralization group (a) and carbonization group (b).

Table 3: Comparison of quantitative results of C_3S content between EBSD and QXRD.

	Remaining amount of C_3S-B (%)	Remaining amount of C_3S-C (%)
QXRD	11.46 ± 1.21	13.42 ± 1.32
EBSD	11.30 ± 1.64	14.10 ± 1.24

consistent, indicating that the data obtained by both characterization methods were reliable.

4. Conclusions

QXRD, TG/DSC, BSE, and FT-IR were used to study the effect of microbial mineralization on the hydration process of C_3S and microstructure of hardened C_3S pastes. The results showed that microbial mineralization promoted the hydration of T-C_3S. QXRD and EBSD/ESD could accurately characterize the content of C_3S, and the differences between the two characterization methods were minute. The content of $Ca(OH)_2$ and $CaCO_3$ at different depths of the sample could be exhaustively analyzed by TG/DSC, and FT-IR could qualitatively characterize the content of $CaCO_3$.

Data Availability

Some or all data, models, or codes that support the findings of this study are available from the corresponding author upon reasonable request.

Conflicts of Interest

The authors declare that they have no conflicts of interest regarding the publication of this paper.

Acknowledgments

The authors appreciate the financial support from the National Natural Science Foundation of China (Grant no.51738003) and the International Cooperation Project supported by Southeast University-Sika Technology AG (8512000478).

References

[1] M. Li, C. Fang, S. Kawasaki et al., "Bio-consolidation of cracks in masonry cement mortars by Acinetobacter sp. SC4 isolated from a karst cave," *International Biodeterioration & Biodegradation*, vol. 141, pp. 94–100, 2019.

[2] J. Zhang, D. Kumari, and V. Achal, "Combining the microbial calcite precipitation process with biochar in order to improve nickel remediation," *Applied Geochemistry*, vol. 103, pp. 68–71, 2019.

[3] D. Kumari, A. Mukherjee, V. Achal, and Q. Zhang, "Biomineralization for sustainable construction - a review of processes and applications," *Earth Science Reviews*, vol. 148, pp. 1–17, 2015.

[4] H. Rong, *Preparation and Binding Mechanism of Microbe Cement*, pp. 44–91, Southeast University, Nanjing, China, 2014.

[5] W. Peiming, F. Shuxia, and L. Xianping, "Research methods and progress of cement hydration," *Journal of Building Materials*, vol. 8, no. 6, pp. 646–652, 2005.

[6] V. Kocaba, E. Gallucci, and K. L. Scrivener, "Methods for determination of degree of reaction of slag in blended cement pastes," *Cement and Concrete Research*, vol. 42, no. 3, pp. 511–525, 2012.

[7] A. V. Soin, L. J. J. Catalan, and S. D. Kinrade, "A combined QXRD/TG method to quantify the phase composition of hydrated Portland cements," *Cement and Concrete Research*, vol. 48, pp. 17–24, 2013.

[8] Z. Basaran Bundur, M. J. Kirisits, and R. D. Ferron, "Biomineralized cement-based materials: impact of inoculating vegetative bacterial cells on hydration and strength," *Cement and Concrete Research*, vol. 67, pp. 237–245, 2015.

[9] J. C. Lee, C. J. Lee, W. Y. Chun, W. J. Kim, and C.-W. Chung, "Effect of microorganism sporosarcina pasteurii on the hydration of cement paste," *Journal of Microbiology and Biotechnology*, vol. 25, no. 8, pp. 1328–1338, 2015.

[10] A. X. S. Bruker, *TOPAS V4: General Profile and Structure Analysis Software for Powder Diffraction data: User's Manual*, Bruker AXS, Karlsruhe, Germany, 2008.

[11] F. Nish, Y. Takeuchi, and I. Maki, "Tricalcium silicate $Ca_3O[SiO_4]$: the monoclinic superstructure," *Zeitschrift für Kristallographie*, vol. 172, pp. 297–314, 1985.

[12] A. Younsi, S. Staquet, and A. A ï T-Mokhtar, "Accelerated carbonation of concrete with high content of mineral additions: effect of interactions between hydration and drying," *Cement and Concrete Research*, vol. 43, pp. 25–33, 2013.